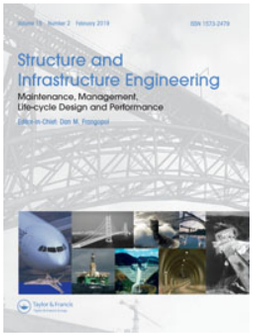

Taylor & Francis
Taylor & Francis Group

Structure and Infrastructure Engineering
Maintenance, Management, Life-Cycle Design and Performance

ISSN: 1573-2479 (Print) 1744-8980 (Online) Journal homepage: https://www.tandfonline.com/loi/nsie20

Effectiveness of passive response control devices in buildings under earthquake and wind during design life

Tathagata Roy & Vasant Matsagar

To cite this article: Tathagata Roy & Vasant Matsagar (2019) Effectiveness of passive response control devices in buildings under earthquake and wind during design life, Structure and Infrastructure Engineering, 15:2, 252-268, DOI: 10.1080/15732479.2018.1547768

To link to this article: https://doi.org/10.1080/15732479.2018.1547768

Published online: 17 Jan 2019.

STRUCTURE AND INFRASTRUCTURE ENGINEERING
2019, VOL. 15, NO. 2, 252–268
https://doi.org/10.1080/15732479.2018.1547768

Effectiveness of passive response control devices in buildings under earthquake and wind during design life

Tathagata Roy and Vasant Matsagar

Multi-Hazard Protective Structures (MHPS) Laboratory, Department of Civil Engineering, Indian Institute of Technology (IIT) Delhi, Hauz Khas, Delhi, India

ABSTRACT

The effectiveness of passive vibration control devices used to retrofit multi-storied steel buildings during their design life is investigated under the dynamic forces induced by earthquake and wind. The passive vibration control devices include steel bracing, viscous and viscoelastic dampers. The buildings without and with the retrofitting devices are modelled as multi-degree of freedom (M-DOF) systems, with inertial masses lumped at each floor level. The governing differential equations of motion for the uncontrolled and controlled buildings are solved using Newmark's time marching scheme. The obtained dynamic responses for the buildings exposed to the earthquake- and wind-induced forces are subsequently compared. It is concluded that upon retrofitting, the modified dynamic properties, such as modal frequencies and damping ratio play an active role to attract forces during the two hazards, which in turn influences the response reduction achieved. It may be worth noting that the buildings retrofitted for earthquake tend to attract more forces under wind load and vice versa. Therefore, a retrofit strategy providing beneficial effects against a particular hazard may prove to be catastrophic for the other, which underlines the need for careful selection of the retrofit solution and design for a structure considering such multi-hazard scenario.

ARTICLE HISTORY
Received 22 August 2017
Revised 6 August 2018
Accepted 10 August 2018

KEYWORDS
Earthquakes; fluid viscous damper; multi-hazard; retrofit; steel bracing; viscoelastic damper; wind

1. Introduction

Extreme natural hazards, such as earthquakes and strong winds, pose significant threat to the socio-economic life causing considerable devastations across the globe (Li et al., 2012; Seible et al., 2008). As a result, the engineering community has been trying to recognize proper assessment techniques to mitigate the increased risk associated with the structure under the multiple hazard scenario. Such increased threats in the structure demand an efficient and advanced assessment strategy. The need for such assessment strategy arises as the existing design codes and guideline standards do not incorporate the holistic approach for all the exposed hazards. Moreover, such approaches are unspoken about the standard risks of exceedance of the structures in regions where both earthquakes and winds occur. The lack of available assessment tools has made it difficult in assessing the structures to confront the future challenges arising from such extreme natural hazards. The application of multi-hazard design to structures will form a potential tool to constitute a resilient community capable of being governed by either loads. The futuristic multi-hazard assessment strategy will outstretch the prevailing methodology to ensure adequate safety and serviceability for structural resistance against such extreme forces. Therefore, the current methodology has been sought to draw the attention of global researchers and concerned personnel to emphasize the necessity of considering the multiple hazard demand in investigating new structural systems as well as retrofit the existing structures.

To develop efficient and fundamental approaches, it is advisable to recognize the distinguished features of the hazards occurring in design life of a structure (Sigtryggsdóttir et al., 2016). These extreme natural threats occurring during the design life of the structure are mutually exclusive and collectively exhaustive events, as the probability of simultaneous occurrence for the hazards is zero. Hence, any structure exposed to multi-hazard scenario under earthquakes and strong winds, experience no more than a particular hazard at each instant of time.

The mutually non-concurrent and independent hazard events have been a significant threat to the civil infrastructures (Aly & Abburu, 2015). Early research exclusively considered the independency of the hazards to assess the safety of structures (Samali & Kwok, 1995; Soong & Spencer, 2000). Thereafter, by the early 21st century, research interest has started developing amongst the researchers and engineers to analyze and design the structures for combinations of such extreme multiple hazards. The emerging multi-hazard assessment concept is a relatively nascent area in structural risk reduction; hence, the multi-risk models available in this area are limited (Komendantova et al., 2014). The unconventional multi-hazard assessment is still in progress, as the existing treatment of multiple hazards in code provisions and design guidelines remains ambiguous (Mahmoud & Cheng, 2016).

CONTACT Tathagata Roy tathagata.roy@civil.iitd.ac.in

Research studies were conducted to establish frameworks for optimal decision-making in mitigating the risks of light-frame wood and high-rise commercial structures under severe windstorms and earthquakes (Cha & Ellingwood, 2013; Li & Ellingwood, 2009). Moreover, the fundamental objectives of multi-hazard assessment were highlighted in modifying the existing design codes and documents for mitigating the additional risks under the strong wind and earthquake scenarios (Duthinh & Simiu, 2010; Potra & Simiu, 2009). In addition, the multi-hazard assessment has been progressing alongside in understanding the performance of lifeline systems and highway networks. Decò and Frangopol (2011) evaluated the risk of highway bridges under the effects of multiple hazards, such as traffic loads, environmental attacks, flood-induced scouring and earthquakes. Akiyama and Frangopol (2013) and Dong and Frangopol (2016) recently assessed the life-cycle performance of highway bridges under time-dependent multi-hazard loading scenario. Yilmaz et al. (2016) developed robust probabilistic tools in assessing the risk of lifeline structures exposed to multiple hazards.

The use of supplemental passive control devices has been gaining notable attention in optimal design and retrofit of structures to distinguish proper mitigation techniques against the multiple hazards. Suitable retrofitting strategies have ensured the safety of structures under the exposure of a particular hazard. Various researchers investigated the effectiveness of retrofitting in building systems under earthquake and wind loads independently (Fur et al., 1996; Matsagar & Jangid, 2005; Mazza & Vulcano, 2011; Patel & Jangid, 2011; Soong & Spencer, 2000). However, code guidelines and design standards are silent regarding the design and retrofit of structures mainly to identify appropriate mitigation techniques under potential hazard combinations. In context with the assessment of retrofitted structures, limited contributions exist in investigating the performance of structures under the multiple hazard scenarios. Dogruel and Dargush (2008) presented a methodology to assess optimal life-cycle of retrofitted structures under seismic and wind excitations. Latest contributions include the investigation of efficiency of retrofitted devices by optimizing the life-cycle cost of the system under the multiple hazard scenarios (Jalayer et al., 2011; Venkittaraman & Banerjee, 2014). The performance and resiliency criteria of the lifeline structures were also enhanced by the retrofitting strategies under the multi-hazard scenario (Chandrasekaran & Banerjee, 2015; Tapia & Padgett, 2016). Nevertheless, the effectiveness of retrofitting in buildings under multi-hazard scenario is yet to be understood appropriately. In addition, it may be observed that a remedial measure for a particular hazard can worsen the response of the structure under other hazard (Roy & Matsagar, 2017). Hence, the ineffectiveness of the retrofitted devices rendered consequently becomes an increased concern for the structural safety under the multi-hazard scenarios.

Herein, this article investigates the performance of the passive control devices under the dynamic earthquake and wind excitations. Herein, assessment of 9-, 20- and 25-storey steel buildings retrofitted with different passive control devices, such as steel bracing (SB), fluid viscous damper (FVD) and viscoelastic damper (VED), is carried out under selected historical earthquake and site-specific wind. The numerical study is conducted to investigate the efficiency of the passive control devices by altering the dynamic properties of the steel buildings under these hazard scenarios. Moreover, the influence of altered dynamic properties of the retrofitted structures on the response quantities is studied. The investigation is also extended to analyze the worsening behavior of the response for the modified dynamic properties against the multi-hazard excitations.

2. Mathematical modelling of building frames

In this study, the mathematical models for the 9-, 20- and 25-storey steel buildings using the passive retrofit devices, such as SBs, FVDs and VEDs are formulated, as shown in Figure 1, and subjected to the dynamic action of earthquake and wind loads. Figure 1(a–d) shows the mathematical model of the considered moment resisting frame (MRF), with the arrangement of retrofit devices. The general assumptions in modelling the buildings with the passive control devices are as follows:

(i) The steel building frames without and with the control devices are modelled as multi-degree of freedom (M-DOF) systems.
(ii) The seismic mass, comprised of structural and non-structural components, is lumped at the joint nodes.
(iii) The floor with the beam–slab interaction is modelled as rigid diaphragm in the direction of the dynamic forces.
(iv) One degree of freedom (DOF) is considered at each floor level in the direction of the dynamic earthquake and wind loads.
(v) The building is modelled with two basement floors, and the horizontal displacement of the first floor is restrained by the surrounding soil and rigid concrete foundation.
(vi) The steel buildings with the control devices are treated as dual systems with the MRFs as primary systems, exhibiting linear behavior and the non-linear control devices, exhibiting elasto-plastic behavior.

The original and retrofitted structures are assumed to remain in elastic range both for earthquake and wind excitations. This is because the study is mainly focused on the characteristics of global response, which considers the linearized response of the structure (Naeim, 1998). Moreover, several recent studies have investigated the effectiveness of various control systems installed in the linear benchmark building (Elias et al., 2017; Raut & Jangid, 2014), which demonstrates a reasonable approximation that can be incorporated in this study.

The mathematical models for the uncontrolled and controlled buildings are obtained, and free vibration analysis is conducted to determine modal periods. Further, the equations are solved using Newmark's time marching scheme,

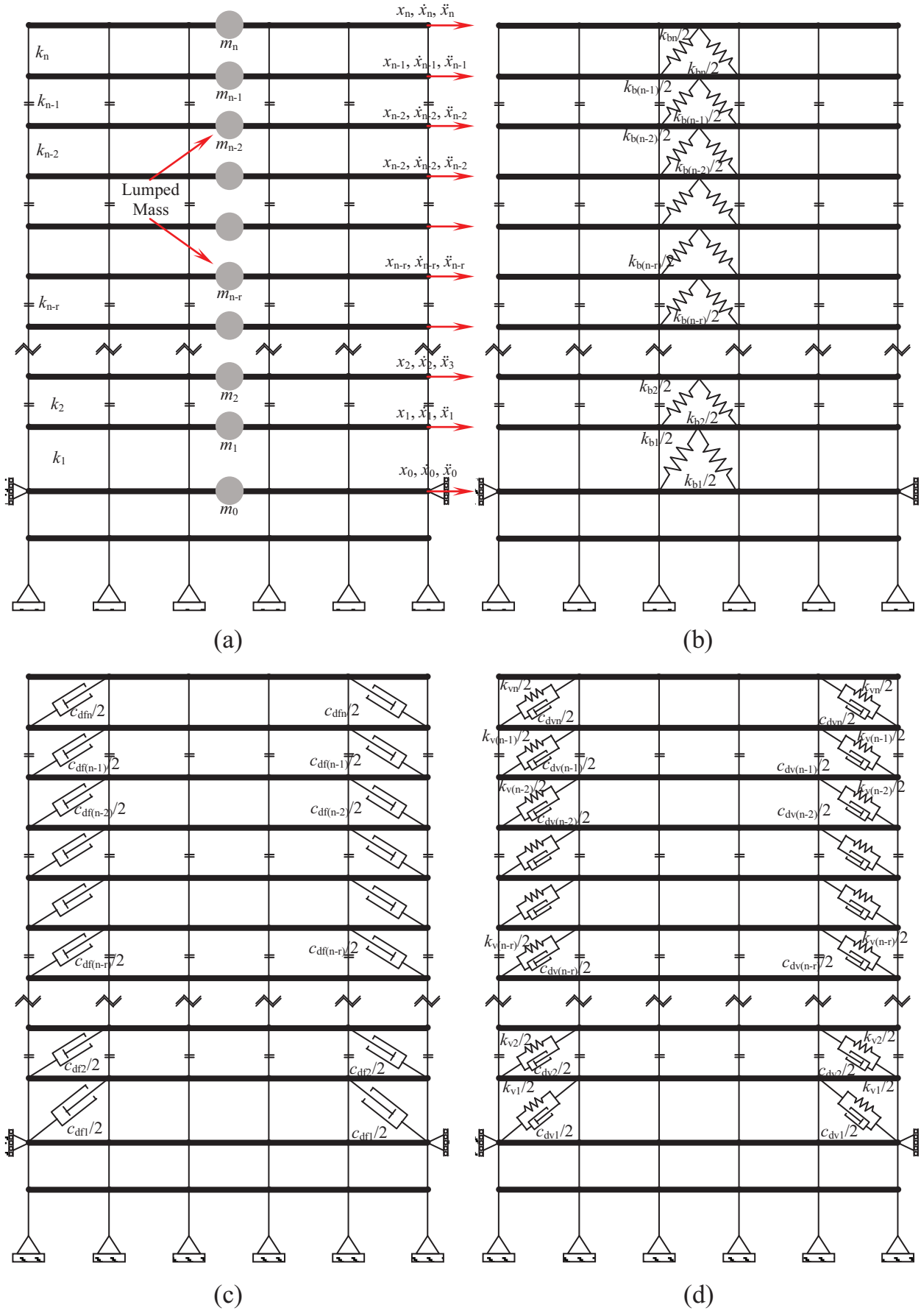

Figure 1. Mathematical model of *n*-storey: (a) steel moment resisting frame (MRF), (b) steel braced frame (SBF), (c) fluid viscous damped frame (FVDF) and visco-elastic-damped frame (VEDF).

with linear acceleration, to obtain the response history for the uncontrolled and controlled buildings.

2.1. Modelling of moment resisting frame (MRF)

The governing differential equation of motion for the MRF buildings is given by:

$$[m]\{\ddot{x}(t)\} + [c]\{\dot{x}(t)\} + [k]\{x(t)\} = p(t) \tag{1}$$

where, $[m]$ is the mass matrix of the model lumped at joint nodes, $[c]$ is the damping matrix, $[k]$ is the stiffness matrix of the building, $\ddot{x}(t)$ is the acceleration response, $\dot{x}(t)$ is the velocity response, $x(t)$ is the displacement response, respectively obtained at each floor of the MRF building, $\{x\} = \{x_1, x_2, x_3, \ldots, x_{n-r}, \ldots x_{n-1}, x_n\}^T$, and $p(t)$ is the external force exerted on the building, in form of the base-excited earthquake or mass-excited wind loads.

For the base-excited seismic ground motions applied as external loads, Eq. (1) is modified as:

$$[m]\{\ddot{x}(t)\} + [c]\{\dot{x}(t)\} + [k]\{x(t)\} = -[m]\{r\}\ddot{x}_g \tag{2}$$

where, $\{r\}$ is the influence coefficient vector, and $\ddot{x}_g$ is the applied earthquake ground motion acceleration. Similarly, when the building is subjected to mass-excited nodal wind loads, Eq. (1) is correspondingly modified as:

$$[m]\{\ddot{x}(t)\} + [c]\{\dot{x}(t)\} + [k]\{x(t)\} = f(t) \tag{3}$$

where, $f(t)$ is the applied force vector at the center of mass of each storey, $\{f\} = \{f_1, f_2, f_3, \ldots, f_{n-r}, \ldots f_{n-1}, f_n\}^T$.

The secondary DOFs, such as vertical DOFs, the DOFs at the spliced locations and the rotational DOFs, are condensed out, and the mass and stiffness matrices are obtained in terms of primary and secondary DOFs which are given as:

$$[\hat{m}] = \begin{bmatrix} \hat{m}_{pp} & \hat{m}_{ps} \\ \hat{m}_{sp} & \hat{m}_{ss} \end{bmatrix}, \text{ and } [\hat{k}] = \begin{bmatrix} \hat{k}_{pp} & \hat{k}_{ps} \\ \hat{k}_{sp} & \hat{k}_{ss} \end{bmatrix} \tag{4}$$

where, $[\hat{m}]$ and $[\hat{k}]$ are the mass and the stiffness matrices obtained after static condensation. Therefore, the reduced damped equation of motion is obtained as:

$$[\tilde{m}]\{\ddot{\tilde{x}}\} + [\tilde{c}]\{\dot{\tilde{x}}\} + [\tilde{k}]\{\tilde{x}\} = \tilde{p}(t) \tag{5}$$

where, $[\tilde{m}] = \{\varphi\}^T[\hat{m}]\{\varphi\}$ is the generalized mass matrix, $[\tilde{c}] = \{\varphi\}^T[\hat{c}]\{\varphi\}$ is the generalized damping matrix, $[\tilde{k}] = \{\varphi\}^T[\hat{k}]\{\varphi\}$ is the generalized stiffness matrix, $\tilde{p}(t) = \{\varphi\}^T\{\hat{p}\}$ is the generalized force vector, $\tilde{x} = \{\varphi\}^T\{x\}$ is the generalized displacement coordinates and $\{\varphi\} = [\tilde{m}]^{-1}[\tilde{k}]$ is the modal matrix. The damping matrix $[\tilde{c}]$ is based on the assumption of the modal damping. The modal damping in each mode is proportionate to the linked frequency. The damping ζ_i in the ith mode is given by:

$$\zeta_i = \min\left\{\frac{\omega_i}{50\omega_1}, 0.1\right\} \tag{6}$$

where, ω_i is the natural frequency at the ith mode.

2.2. Modelling of steel braced frame (SBF)

Steel concentric-braces (CBs) provide an effective retrofit approach to achieve the lateral stiffness and prevent relative drift in a vibrating system. In addition, these devices absorb large energy through hysteretic cycles and strength required for advanced seismic design provisions (Kaur et al., 2012). The behavior of steel CBs in both the elastic and plastic ranges determines the global behavior of such structural systems (Chao et al., 2013). The yield displacement and lateral stiffness of the CBs indicate the design parameters for such assemblages, calculated from storey stiffness.

Therefore, considering all the design parameters, the SBs are modelled following the assumptions: (1) the SBs are prevented from yielding in tension, however, may buckle in compression, and (2) the in-plane stiffness of the metallic braces is considered and out-of-plane stiffness is neglected. The CBs are modelled as truss elements to transfer the lateral seismic or wind loads as compression or tension.

Hence, the generalized governing differential equation of motion (Eq. (5)) for the SBF is modified with the change in lateral stiffness, $[\tilde{k}']$, where, $[\tilde{k}'] = [\hat{k}'] + [k_b \cos^2\theta]$ is the stiffness imparted by the columns and the steel braces of the buildings (k_b); and θ is the horizontal angle subtended between the steel brace and beam. For the considered configuration of the steel braces in the MRF, the axial stiffness k_b is represented in terms of the material and geometric properties as:

$$k_b = \frac{EA}{L} \tag{7}$$

where, E is the modulus of elasticity for the steel, A is the cross-section area of the brace and L is the effective length of the brace.

2.3. Modelling of fluid viscous damped frame (FVDF)

The non-linear FVD follows the Newtonian model corresponding to the force proportional to the fractional power law of velocity. The range of the non-linearity affects the force-deformation loop as described by different researchers, namely, Lee and Taylor (2001) and Martinez-Rodrigo and Romero (2003). Therefore, the non-linear force-velocity behavior of the FVD is given by:

$$f_{df} = [c_{df}]|\dot{x}|^{\alpha}\text{sgn}|\dot{x}| \tag{8}$$

where, f_{df} is the output viscous damping force, c_{df} is the damping coefficient obtained from the non-linear FVD, the exponent α depends on the viscosity of the fluid ranging from 0.2 to 1, $\dot{x}$ is the relative velocity between the two ends of damper; sgn represents the symbolic function.

The governing differential equation of motion for the FVDF, incorporating the non-linear force-velocity behavior under the dynamic loads, is expressed as:

$$[\tilde{m}]\{\ddot{\tilde{x}}\} + [\tilde{c}]\{\dot{\tilde{x}}\} + [\tilde{k}]\{\tilde{x}\} + f_{df} = \tilde{p}(t) \tag{9}$$

where, $[\tilde{c}'] = [\tilde{c}] + [c_{df}\cos^2\theta]$ is the equivalent structural damping obtained from the viscous damping of the non-linear FVD, while $[c_{df}] = 2\zeta_{df}[\tilde{m}]\{\omega_n\}$ is the damping matrix

obtained from the supplemental damping, ζ_{df} is assumed to be 5–30% of the critical damping, best results obtained with around 15–20%.

2.4. Modelling of viscoelastic damped frame (VEDF)

The VED holds the advantage of both spring and dashpot effects to restrict excessive vibrations induced from the extreme earthquake and wind forces. The mechanical models of the VED comprise of spring and dashpot in series or parallel to describe the rheological properties of the VED, as described by Lewandowski and Pawlak (2011). In this study, the dynamic performance of VED is described by the fractional Kelvin–Voigt model (spring-dashpot in parallel combination). The non-linear force-deformation behavior is modelled as:

$$f_{dv} = k_v x^{\beta} + c_{dv}\dot{x}^{\alpha} \tag{10}$$

where, f_{dv} is the output viscoelastic damping force; k_v is the axial stiffness of the VED; c_{dv} is the damping obtained from the VED; α and β are the non-linear exponents of the damping and the stiffness, respectively.

Hence, the governing differential equation of motion for the viscoelastic damped frame, which includes the non-linear force-deformation behavior of the damper under the earthquake and wind loads, is given by:

$$[\tilde{m}]\{\ddot{\tilde{x}}\} + [\tilde{c}]\{\dot{\tilde{x}}\} + [\tilde{k}]\{\tilde{x}\} + f_{dv} = \tilde{p}(t) \tag{11}$$

where, $[\tilde{k}'] = [\hat{k}'] + [k_b \cos^2\theta]$ is the stiffness of the building imparted by the columns and the VED; whereas, $[\tilde{c}'] = [\tilde{c}] + [c_{df} \cos^2\theta]$ is the equivalent structural damping obtained from the viscoelastic damping. And, $[c_{dv}] = 2\zeta_{dv}[\tilde{m}]\{\omega_n\}$ is the damping matrix obtained from the supplemental damping.

It can be noted that the FVD and VED are not designed for installing it into the buildings. There are standard design procedures for FVD and VED. The critical parameters for design of an FVD are damping coefficient obtained from the non-linear FVD (c_{df}) and the exponent α, whereas, the design variable for a VED is frequency and temperature dependent dynamic stiffness, which are generally defined in terms of experimentally obtained shear storage modulus and the shear loss modulus.

To select the appropriate values for design procedure, an iterative procedure is required for optimal placement and degree of strengthening to achieve a target damping ratio (Heydarinouri & Zahrai, 2017). Since the focus of the research is not to retrofit a damaged structure for upgrading it to a specific performance level; no such iterative design is performed here. Some practical extemporary design parameters are assumed for retrofitting the buildings using FVD and VED and behavior of the retrofitted structures thus achieved is compared under the multi-hazard scenarios of earthquake and wind.

3. Multiple hazard scenarios

3.1. Earthquake hazard

Early research used stochastic models to generate earthquake loads using empirical or physical models. These seismic hazards are primary functions of spectral acceleration, duration of excitation, frequency content of the ground motions, etc. Ground motions play an important role in assessing the dynamic response of structures, as great variation of response occurs with a slight change in ground motion (Roy & Agarwal, 2016). Hence, specific numbers of well-known historical earthquakes are considered for the analysis with appropriate ground motion characteristics.

Near-field and far-field earthquakes are considered based on their widespread research in terms of the structural impact. The earthquakes are chosen according to their frequency content, distinguishing into narrow- and broad-band based on the range of dominating frequency. Moreover, in order to utilize the advantages of these time-history data of real earthquake ground motions to analyze the structures, one of the several issues that warrant addressing is the scaling issue. The scaling of earthquakes is primarily done to: (1) investigate the extent of non-linearity for different earthquakes at different intensity measure (IM) levels, (2) to investigate probability of damage for different levels of the IM levels and (3) to carry out experimental investigation of prototype structure using shake table test.

The scaling factors may be arrived at by using different methodologies (Kalkan & Chopra, 2010; Mazza & Labernarda, 2017). In this work, neither the effect and extent of non-linearity nor the probability of damage for different earthquakes at different IM levels have been studied. Moreover, no experimental studies have been covered in this topic. In this research, only the responses of the uncontrolled and controlled structures are compared under the assumption that the retrofitted structures are considered to remain in elastic range both under the multi-hazard scenario of earthquake and wind-induced forces.

It should also be noted that the assumption of few seismic ground motion loadings may not be viable to stamp an authority on the range of results and in-depth conclusions obtained. However, the proposed idea would help to acquire distinct knowledge on the current multi-hazard scenario and focus on the holistic approach to create a hazard resilient society.

3.2. Wind hazard

The wind hazard at a location is expressed as a function of the maximum wind speed for the site followed by the gust factor. In many design codes and building standards of wind loading, a peak gust speed, $U_{3s\text{-}10}$ (3-second gust speed at 10 m height from the ground) is used to calculate the design wind loads. To address the multi-hazard effect on the steel buildings, site-specific wind loadings are considered. The non-concurrent along wind loadings are considered for the same site as the earthquake loadings.

Table 1. General properties for the *n*-degree of freedom (*n*-DOF) system of the moment resisting frame (MRF) building.

No. of storeys	Storey levels	Seismic mass, m_n (kg)	Stiffness, k_n (kN/m)	Damping, c_n (kN-s/m)	Dimension (m)
9-storey	Basement (n_b)	–	–	–	3.65
	Ground (n_0)	4.83×10^5	77.87×10^3	2.08×10^5	5.49
	1st (n_1)	5.05×10^5			3.96
	2nd (n_2) - 8th (n_8)	4.95×10^5			3.96
	9th (n_9)	5.35×10^5			–
	Bay widths	–	–	–	9.15
20-storey	Basement (n_b)	–	–	–	3.65
	Ground (n_0)	2.66×10^5	2.75×10^5	8.55×10^4	5.49
	1st (n_1)	2.83×10^5			3.96
	2nd (n_2)–19th (n_{19})	2.76×10^5			3.96
	20th (n_{20})	2.92×10^5			–
	Bay widths	–	–	–	6.10
25-storey	Basement (n_b)	–	–	–	3.65
	Ground (n_0)	2.66×10^5	2.35×10^5	5.60×10^4	5.49
	1st (n_1)	2.83×10^5			3.96
	2nd (n_2)–24th (n_{24})	2.76×10^5			3.96
	25th (n_{25})	2.92×10^5			–
	Bay widths	–	–	–	6.10

The wind loads, with static and fluctuating components, are simulated from NatHaz online wind simulator (NOWS): simulation of Gaussian multivariate wind fields (Kwon & Kareem, 2006). The simulation technique involves obtaining discrete frequency function with Cholesky decomposition and fast Fourier transform (FFT) for wind speed, which is considered as the wind hazard parameter here. The time histories of the wind speeds are obtained thereafter by summing the static and fluctuating components obtained from the simulation based on Bernoulli's theorem, given as under:

$$\bar{U}(t) = 0.5\rho C_d A[U(t) + u(t)]^2 \tag{12}$$

where, ρ is the air density, C_d is the drag coefficient depending on the shape of the object, A is the exposed area, $U(t)$ is the mean speed component and $u(t)$ is the fluctuating speed component of the wind time history.

4. Numerical study

In this study, effectiveness of the passive control devices installed in 9-, 20- and 25-storey steel buildings is investigated under the dynamic earthquake and wind loads. The 9- and 20-storey benchmark steel buildings are modelled and analysed with the passive control devices for further investigation (Ohtori et al., 2004; Spencer et al., 1999). In addition to the 9- and 20-storey buildings, a 25-storey building is similarly designed for the gravity loads by extending the stories of the 20-storey benchmark steel building and checked against the limit states of collapse and serviceability.

Retrofitting of the steel buildings is carried out by adding either stiffness and/or damping. The proportional stiffness for the passive control devices assumed is 60% of the storey stiffness and the proportional damping assumed is $\zeta = 15\%$ of the critical damping. The non-linear exponent α for the FVD as well as the VED is assumed as 0.3. The non-linear exponent of the stiffness, β, is assumed as 2 to simulate classical Kelvin–Voigt model for the non-linear VED.

The material and geometric properties assumed for this study are shown in Table 1. Free vibration analysis is performed for the uncontrolled and controlled buildings and the results are obtained in terms of natural periods given in Table 2 as under. The multi-hazard assessment for the 9-, 20- and 25-stories is conducted under four historical earthquakes: (1) the NS component of the El Centro earthquake recorded at Imperial Valley Irrigation District substation in El Centro, California on 18th May 1940, (2) the 90 component of the Loma Prieta earthquake recorded at Los Gatos Presentation Center (LGPC) station on 18th October 1989, (3) the NS component of the Northridge earthquake recorded at Sylmar County Hospital parking lot in Sylmar, California on January 17th 1994 and (4) the NS component of the Kobe earthquake recorded at Japanese Meteorological Agency (JMA) station on 17th January 1995. Response spectrum of ground motion acceleration and displacement is plotted for the selected earthquakes to demonstrate the nature of the responses obtained for the steel buildings, as shown in Figure 2.

Table 2. Modal analysis results for the *n*-DOF system in terms of period (s).

	MRF	SBF	FVDF	VEDF
9-storey	2.88	2.19	2.88	2.17
	1.01	0.68	1.01	0.64
	0.61	0.35	0.61	0.33
	0.42	0.23	0.42	0.22
	0.32	0.18	0.32	0.16
20-storey	3.86	3.12	3.86	3.11
	1.33	0.98	1.33	0.94
	0.78	0.53	0.78	0.49
	0.55	0.35	0.55	0.33
	0.42	0.26	0.42	0.25
25-storey	5.88	4.68	5.88	4.86
	2.15	1.48	2.15	1.49
	1.25	0.74	1.25	0.76
	0.89	0.46	0.89	0.50
	0.68	0.32	0.68	0.37

The wind hazard incorporated in the study are simulated from the NatHaz online simulator with gust speed as 33, 39, 46 and 55 m/s located in urban and suburban areas with numerous closely spaced obstructions (Category-B) having cut-off frequencies obtained from the free vibration analysis of the building frames. The gust wind speeds are noted from the regions of interest where multiple hazard scenarios exist, such as California region of the USA and South-East Coast of Japan. Design wind speed for the California region

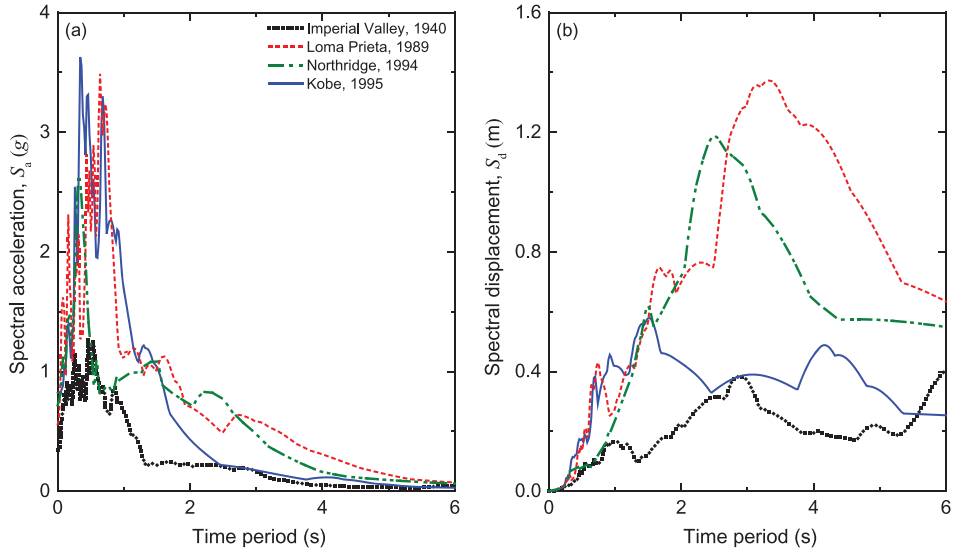

Figure 2. Response spectrum of the selected earthquakes for: (a) ground motion acceleration and (b) ground motion displacement.

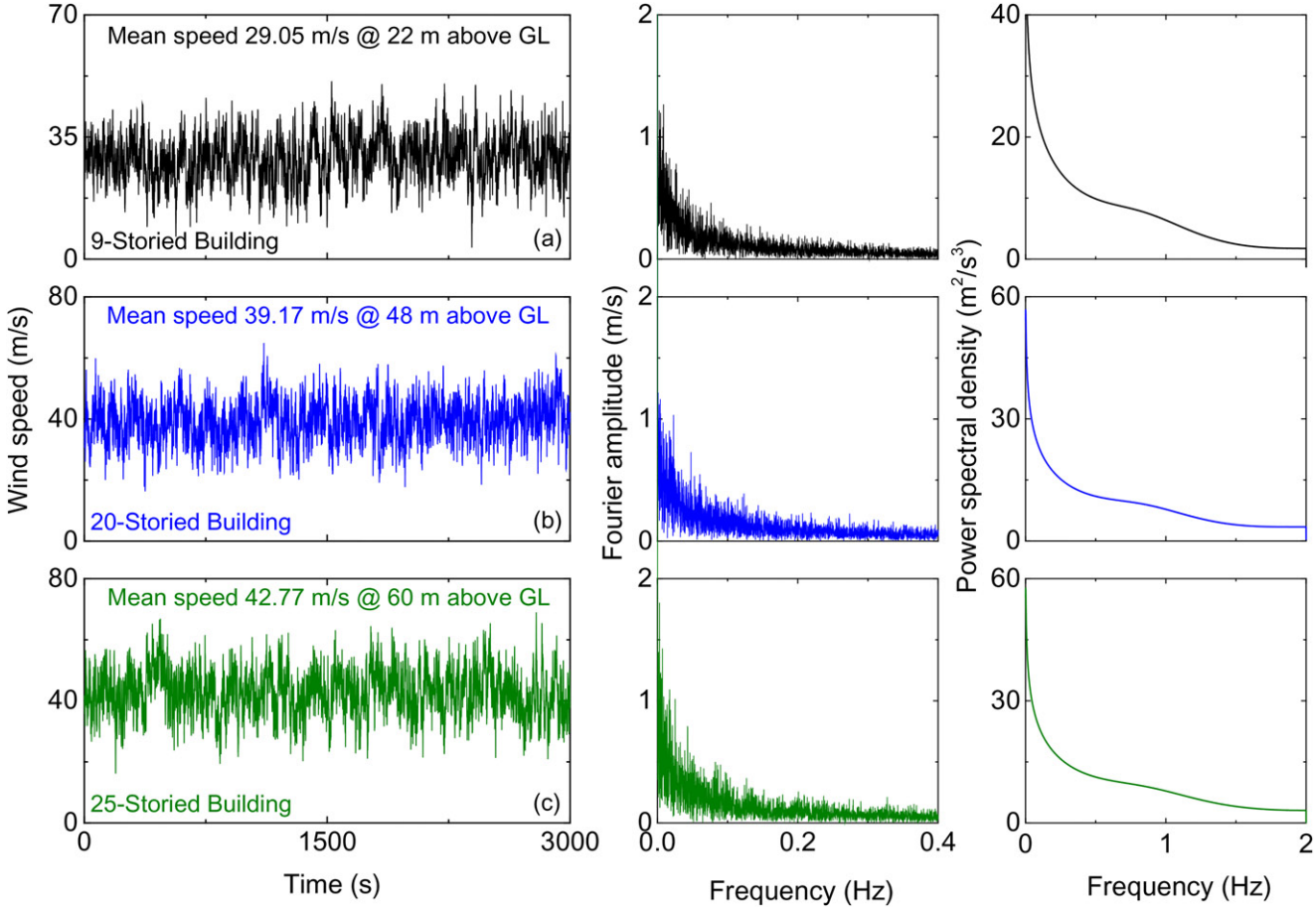

Figure 3. Wind speed at a specific height for the: (a) 9-storey, (b) 20-storey, (c) 25-storey along with the frequency content (FFT spectra) and power spectral density (PSD).

is 39 m/s; whereas for the South-East Coast of Japan, the design speed is 46 m/s.

However, the other wind speeds are assumed based on Indian standard code to maintain a comparability amongst the parameters. Time history of the wind excitation with gust speed 46 m/s along with the corresponding FFT and power spectral density (PSD) for the steel buildings, plotted in Figure 3(a–c). The FFT and PSD spectra refer to the frequency and energy content in the considered wind loads, essential in evaluating the nature of the structural responses under the gusty wind loads.

Tables 3 and 4 highlight the details of considered earthquakes and winds used in the study. Response quantities, such as top floor acceleration ($\ddot{x}_n$, $n = 9$, 20 or 25), inter-storey

drift (δ), base shear (V_b) and top floor displacement (x_n, $n = 9$, 20 or 25), are chosen to address the multi-hazard consequence for the steel buildings. The floor accelerations developed in the superstructure are proportional to the force exerted by the structures under the dynamic earthquake and wind excitations and also determine the serviceability criteria (e.g. comfort level of occupants) of the structures. The displacement as well as the inter-storey drift ratio is influential in determining the design of the lateral load carrying components of the structural systems.

Table 3. General characteristics of the historical earthquake loadings used in the study.

Sl. no.	Earthquake	Event date	Recording station	Component	PGA (*g*)
1	Imperial Valley	18th May 1940	El Centro	00	0.34
2	Loma Prieta	18th October 1989	LGPC	360	0.55
3	Northridge	17th January 1994	Sylmar	NS	0.83
4	Kobe	17th January 1995	JMA	90	0.82

Table 4. General characteristics of the site-specific wind excitations used in the study.

Sl. no.	Gust wind speed (m/s)	Cut off frequency (Hz)	Exposure category	Duration (s)
1	33	0.5	B	2000
2	39			
3	47			
4	55			

4.1. Deterministic study for 9-storey steel buildings

The effectiveness of retrofitting systems for the 9-storey benchmark steel buildings is investigated from the response history data for the chosen parameters under the multi-hazard scenario. Table 5 shows the peak response for the 9-storey steel building frames without and with the passive control devices under the considered earthquakes, whereas Table 6 highlights the peak responses for the wind excitations. Figure 4 presents the distribution of the peak responses for the 9-storey steel building under the multiple hazard scenarios of earthquake and wind.

Under the seismic excitations, the peak top floor acceleration ($\ddot{x}_*$) and base shear (V_b) for the SBF are the highest. With decreased modal periods, the SBF attracts large forces owing to relative stiffness, as observed from the plot of response spectrum (Figure 2). On the other hand, the

Table 5. Comparison of the peak response for the different steel building systems under real-time earthquake loadings.

	Response quantities	Top floor acceleration, $\ddot{x}_n$ (m/s^2)			Inter-storey drift, δ (%)			Base shear, V_b ($\times 10^3$ kN)			Top floor displacement, x_n (m)		
Events	No. of storeys	9	20	25	9	20	25	9	20	25	9	20	25
Imperial Valley, 1940	MRF	6.535	2.503	3.374	1.859	0.635	1.473	3.969	3.396	0.325	0.351	0.364	0.483
	SBF	7.274	4.782	4.351	0.854	0.751	0.614	7.026	8.256	0.560	0.195	0.493	0.261
	FVDF	3.643	2.885	2.984	0.807	0.327	0.507	1.768	2.815	0.319	0.206	0.209	0.191
	VEDF	5.632	3.285	3.119	0.407	0.338	0.322	3.521	3.915	1.382	0.103	0.236	0.169
Loma Prieta, 1989	MRF	12.782	11.092	9.691	3.964	1.110	3.893	9.466	19.019	0.720	0.977	1.819	1.328
	SBF	18.831	10.551	8.545	3.387	3.307	4.240	37.168	27.213	1.251	0.971	1.917	1.855
	FVDF	8.858	5.187	7.070	2.407	1.450	2.357	6.698	9.300	0.661	0.677	0.923	0.921
	VEDF	10.367	5.755	3.712	1.306	1.743	1.939	17.708	15.959	3.229	0.393	0.945	0.918
Northridge, 1994	MRF	16.582	7.138	9.608	4.616	1.702	3.915	13.649	11.143	0.815	1.438	1.036	1.024
	SBF	17.287	8.254	12.015	2.586	1.814	2.832	22.944	19.512	1.333	0.795	1.381	1.034
	FVDF	11.734	5.749	6.792	2.303	1.450	2.016	5.464	10.892	0.713	0.695	0.591	0.681
	VEDF	11.102	6.922	4.005	1.523	1.158	1.664	16.771	9.897	3.745	0.495	0.734	0.345
Kobe, 1995	MRF	8.097	7.588	11.115	4.911	1.401	3.096	10.674	10.913	0.768	0.691	0.549	0.571
	SBF	11.288	10.591	11.920	2.678	2.168	2.648	24.274	17.475	1.526	0.731	0.578	0.721
	FVDF	6.903	5.771	8.446	2.006	0.868	1.103	4.562	6.698	0.689	0.417	0.449	0.277
	VEDF	7.725	5.117	9.090	1.296	1.665	0.956	17.523	11.251	4.015	0.349	0.403	0.356

Table 6. Comparison of the peak response for the different steel building systems under site-specific wind loadings.

	Response quantities	Top floor acceleration, $\ddot{x}_n$ (m/s^2)			Inter-storey drift, δ (%)			Base shear, V_b (kN)			Top floor displacement, x_n (m)		
Events	No. of storeys	9	20	25	9	20	25	9	20	25	9	20	25
33 m/s	MRF	0.037	0.140	0.214	0.046	0.203	0.289	0.094	0.755	1.221	0.009	0.096	0.282
	SBF	0.022	0.162	0.278	0.024	0.147	0.169	0.157	0.981	1.719	0.005	0.061	0.167
	FVDF	0.007	0.132	0.228	0.045	0.186	0.239	0.092	0.492	1.197	0.008	0.086	0.271
	VEDF	0.005	0.178	0.261	0.039	0.157	0.186	0.105	0.420	0.949	0.007	0.053	0.152
39 m/s	MRF	0.042	0.191	0.331	0.067	0.251	0.383	0.132	1.086	1.854	0.016	0.143	0.413
	SBF	0.051	0.219	0.272	0.031	0.163	0.181	0.202	1.234	2.104	0.006	0.087	0.268
	FVDF	0.018	0.178	0.346	0.058	0.237	0.315	0.118	0.751	1.530	0.010	0.138	0.382
	VEDF	0.013	0.233	0.303	0.049	0.181	0.239	0.141	0.734	1.197	0.008	0.062	0.241
46 m/s	MRF	0.105	0.289	0.392	0.076	0.347	0.791	0.182	1.816	2.906	0.024	0.213	0.588
	SBF	0.097	0.288	0.406	0.035	0.223	0.434	0.249	1.992	3.027	0.010	0.147	0.357
	FVDF	0.090	0.244	0.392	0.066	0.290	0.590	0.148	1.536	2.457	0.021	0.178	0.456
	VEDF	0.051	0.313	0.390	0.055	0.207	0.466	0.201	1.146	1.834	0.013	0.133	0.296
55 m/s	MRF	0.127	0.403	0.432	0.105	0.430	1.060	0.258	2.227	3.564	0.037	0.267	0.790
	SBF	0.109	0.496	0.462	0.047	0.273	0.588	0.312	2.307	3.692	0.014	0.184	0.520
	FVDF	0.102	0.264	0.432	0.086	0.369	0.909	0.191	1.954	3.127	0.028	0.228	0.668
	VEDF	0.072	0.558	0.442	0.081	0.249	0.466	0.270	1.416	2.266	0.016	0.166	0.492

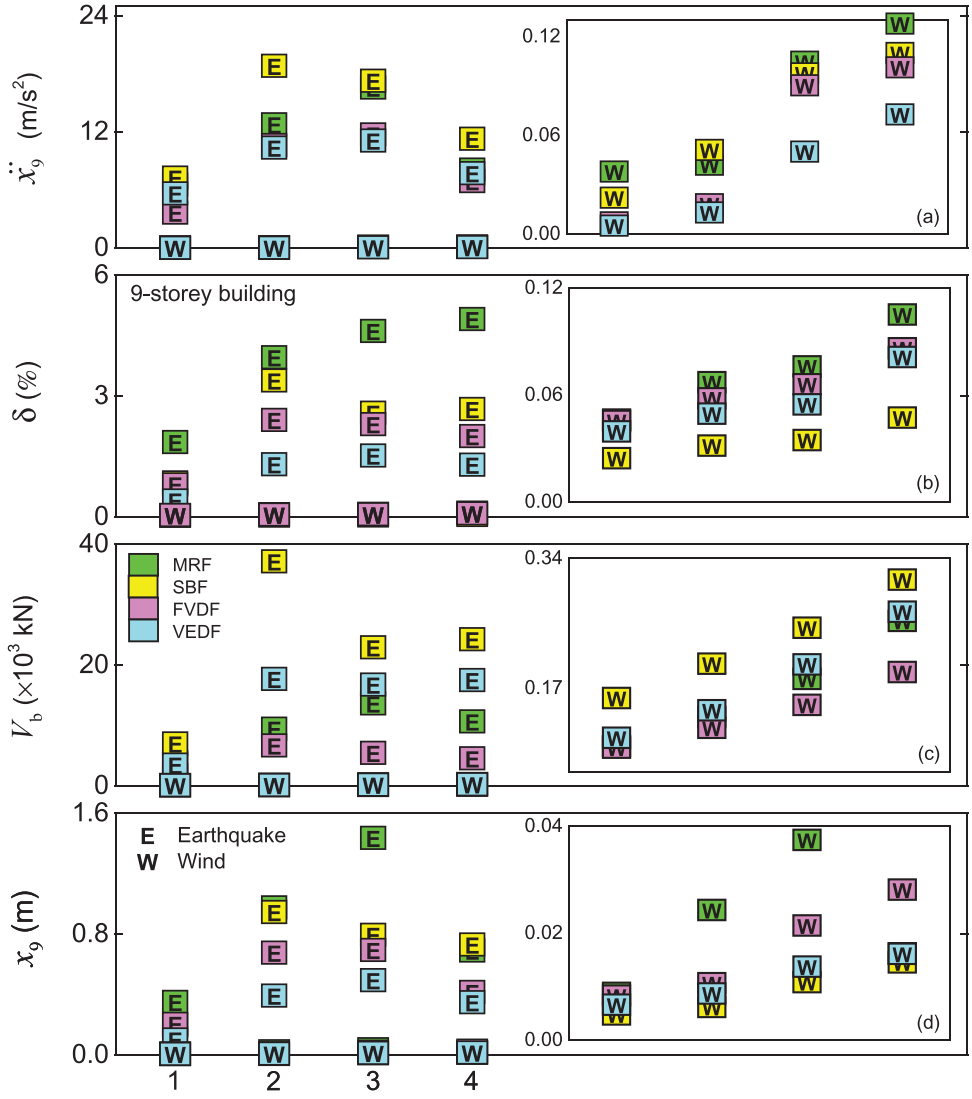

Figure 4. Distribution of the peak load of responses for the 9-storey steel building under the multiple hazard scenarios of earthquake and wind.

additional damping induced FVD and VED are most efficient in dissipating the seismic energy as observed for the inter-storey drift (δ) and displacement response (x_*). Overall, the retrofitted control devices equipped with additional damping are effective in reducing the large seismic responses; in most cases, the least response is observed in the VEDF due to the effect of additional stiffness and damping.

The response quantities observed under the wind excitations are noticeably low as compared to the response obtained under the earthquakes. The wind responses are magnified to demonstrate the variation in distribution under different gusty along wind excitations. The installed passive control devices are capable to reduce the wind responses, as the additional damping induced FVDF and VEDF are observed to have significant reduced response for top floor acceleration ($\ddot{x}_*$) and column base shear. The VEDF, having combined advantage of additional stiffness and damping, results in significant response reduction under the wind loads. The reduced response is obtained from the combined action of non-linear stiffness and damping component, which accounts for increased energy dissipation as compared to the other two retrofitting schemes. Moreover, the SB is observed to be effective in controlling the inter-storey drift (δ) and displacement response (x_*).

Therefore, it is concluded that the additional damping characterized retrofit devices, such as the FVD and VEDF, are efficient in reducing the dynamic earthquake response, while the stiffness characterized retrofit device, as the SBF is effective in reducing the wind response due to the change in dynamic properties under the multiple hazards. It may be implicit to conclude that the retrofit strategies preferred to minimize the large responses for a particular hazard (here earthquake) may be unsuitable to control the responses against the other hazard (here wind). Hence, in such cases, an accurate approach is required to be enforced, which calls for a careful selection of the retrofit solution considering the multi-hazard scenario.

4.2. Deterministic study for 20-storey steel buildings

Herein, the effectiveness of the considered passive retrofit devices is studied for the 20-storey benchmark steel frame buildings under the multiple hazard scenarios of dynamic earthquake and wind excitations. Table 5 depicts the peak response for the 20-storey steel building frames without and

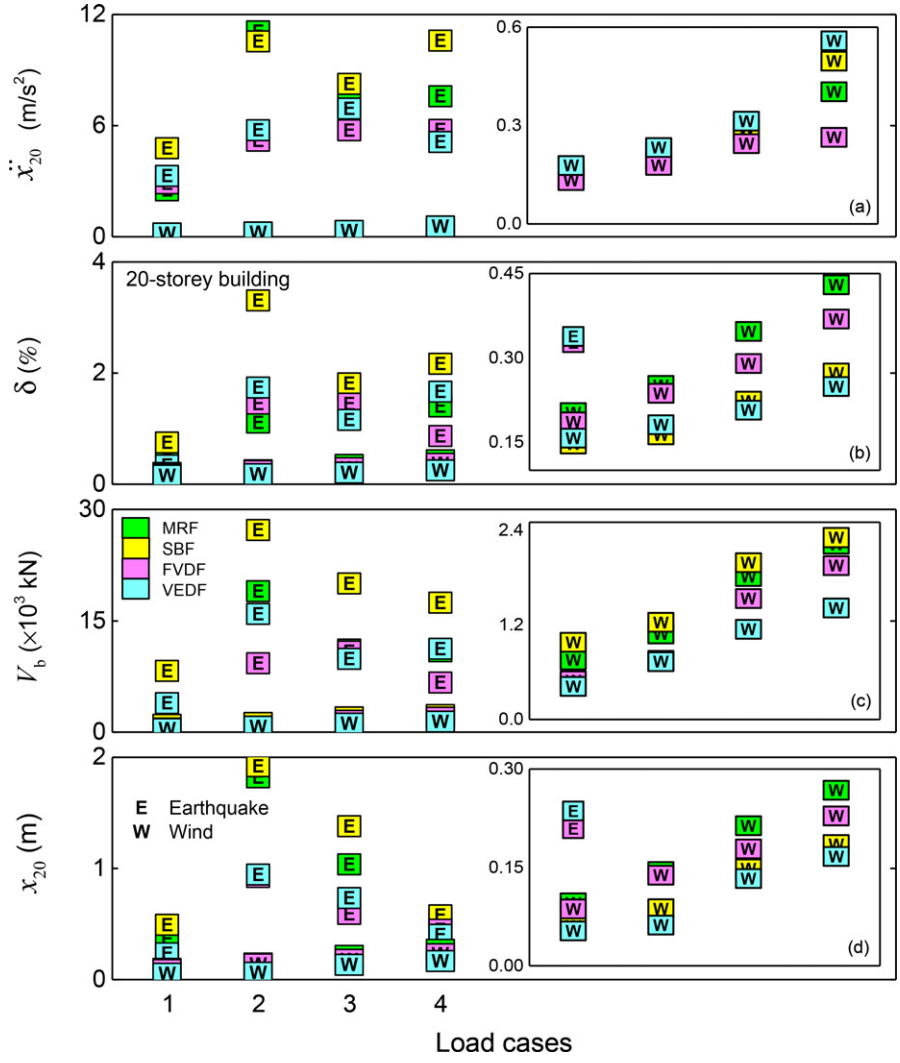

Figure 5. Distribution of the peak load of responses for the 20-storey steel building under the multiple hazard scenarios of earthquake and wind.

with the passive control devices under the considered earthquakes, whereas Table 6 highlights the peak responses for the winds. Figure 5 illustrates the distribution of the peak load of responses for the 20-storey steel building under the multiple hazard scenarios of earthquake and wind. The figure can be used to understand the difference in the responses induced by the earthquake and wind forces. The highest response, observed for the SBF, is invariably for all the considered response quantities. This indicates that the SBF is vulnerable under the horizontal seismic excitations, attracting large forces. On the other hand, the FVDF and VEDF are observed to have the least response, owing to the enhanced effectiveness by additional damping.

The wind responses for the 20-storey steel buildings are comparatively insignificant; however, increased as compared to the 9-storey buildings. The variations in distribution of the wind responses are shown in the adjacent plots to illustrate the effectiveness of the control devices. It may be observed that the acceleration ($\ddot{x}_*$) and base shear (V_b) responses are increased significantly on installing the additional stiffness induced SB and VED. However, there is a significant reduction in inter-storey drift (δ) and top floor displacement (x_*) responses for the SBF and VEDF.

The additional stiffness induced control devices (SB and VED) have substantial contribution in response reduction under the considered wind loads. Addition of stiffness has major influence in the reduction of response against the mass-excited wind loads, due to the lower frequency content in the time-varying loads (Figure 3). The discussion, therefore, highlights that the stiffness induced control devices, SBF and VEDF, are inefficient in seismic response control due to the change in dynamic properties.

Nonetheless, such control devices are truly capable of reducing the wind response, as the modified properties turn in favor of the wind response. In the contrary, the additional damping added devices, the FVDF and VEDF, have considerable seismic response reduction, which cause significant decay in the large responses of the earthquakes by dissipating the energy induced in the structure. This added damping, whatsoever, has insignificant response reduction under the dynamic wind scenario. Therefore, it becomes a demanding task to form a judgmental notion in selecting a retrofit device for the structures prone to

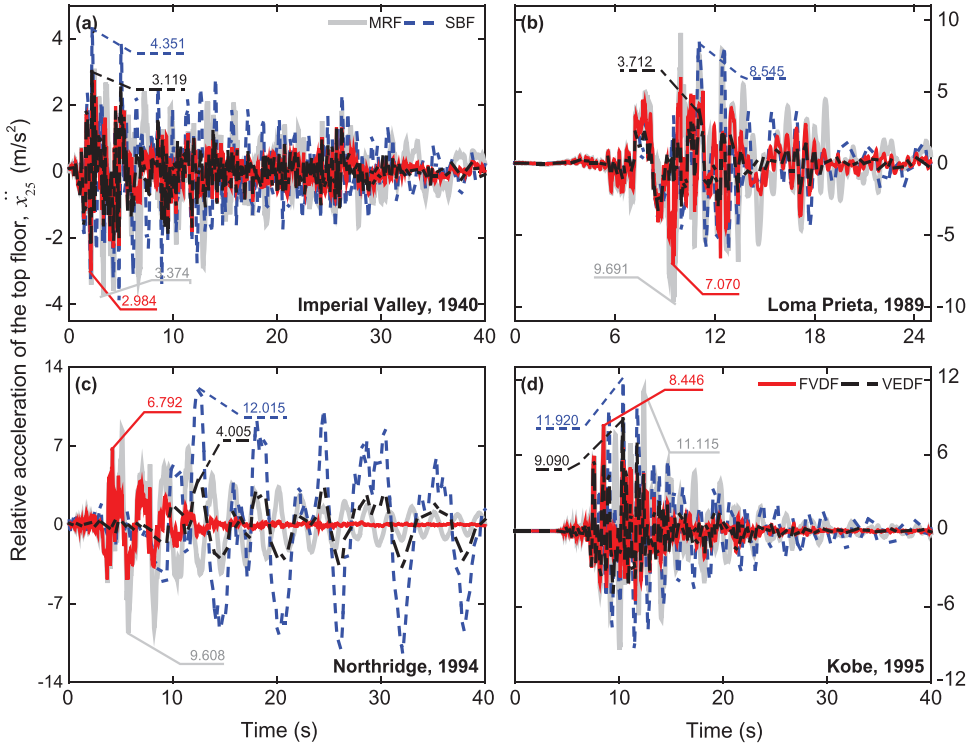

Figure 6. Relative acceleration of the top floor for 25-storey steel building under the considered earthquakes.

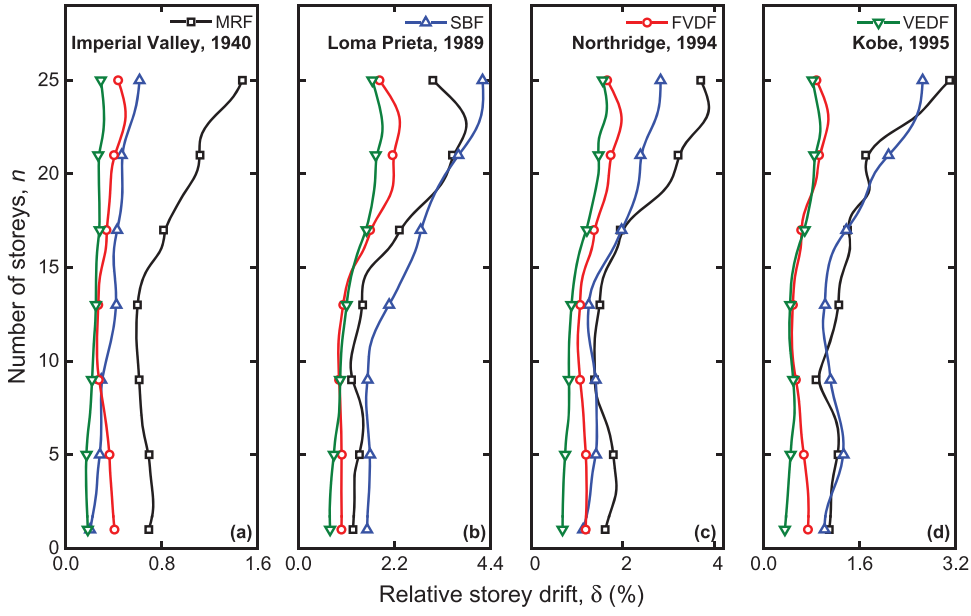

Figure 7. Relative inter-storey drift for the 25-storey steel building under the selected earthquakes.

devastating effects of predominant multiple hazards as earthquake and wind.

4.3. Deterministic study for 25-storey steel buildings

The multi-hazard assessment is conducted for the 25-storey steel buildings controlled with the passive devices by extending the 20-storey benchmark building and is highlighted in Tables 5 and 6. The relative peak responses are investigated as shown in Figures 6–11. The acceleration response ($\ddot{x}_*$) of the top floor is studied under the multiple hazard scenarios of earthquakes and winds. From Figure 6, it is observed that retrofitting by the SB has adverse effect on the response of the structure, thereby increasing the response significantly under the earthquakes. The highest response is noticed for the SBF for most of the earthquake ground motion scenarios. The least response is observed for the additional damping induced control devices, as the FVDF and VEDF.

The inter-storey drift (δ) is considered to investigate the effectiveness of the passive devices under the multiple loading scenario of earthquakes and winds, as shown in Figure 7. It is evident that the use of the SB tends to increase the

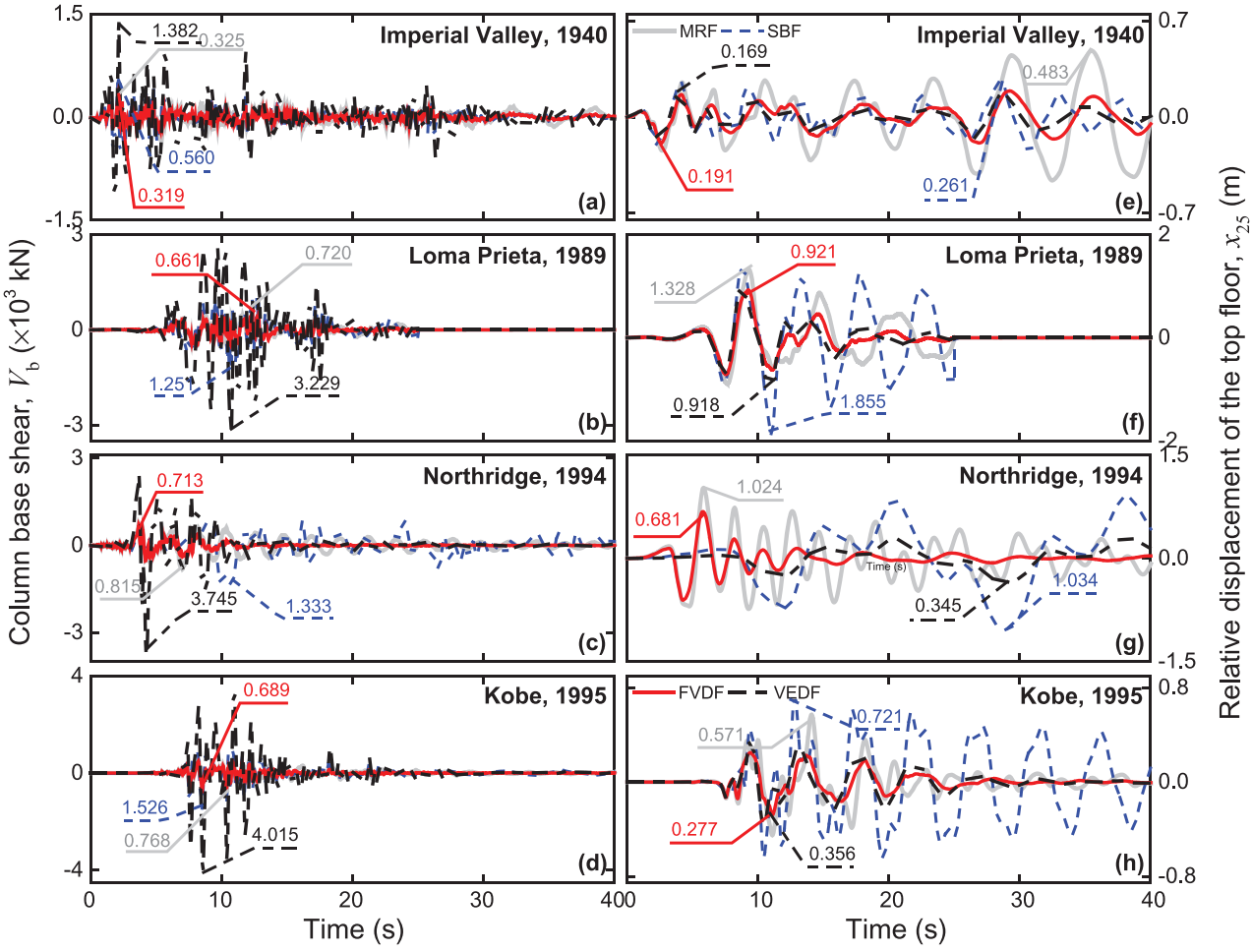

Figure 8. Base shear and relative displacement of the top floor for 25-storey steel building under the considered earthquakes.

inter-storey drift under the earthquake events. It is inasmuch as the higher modes participate in the contribution of the response, leading to an increased response under the modified dynamic properties of the buildings. The least response is identified for the added stiffness and damping induced VEDF building under all the seismic events. The supplemental damping along with the stiffness assists in significant energy dissipation, resulting in reduced response.

As shown in Figure 8(a–d), the base shear (V_b) response chosen to quantify the multi-hazard situation does not follow the trend for the above-discussed cases under the seismic ground motions. Interestingly, there is a significant increase in the response is observed for the VEDF and is calculated to be the highest, although the added stiffness and damping has the tendency to decrease the response. The top floor displacement (x_*) response is similarly considered to investigate the efficiency of the passive devices. Figure 8(e–h) shows the relative displacement of the top floor under the considered earthquakes, which has clear representation of the variation of responses for the retrofitting solutions. The response is the highest for the SBF under the considered earthquakes. The least floor displacement is observed for the VEDF.

The wind forces have significant effect on the responses, as the building is sensitive to the wind forces, however, earthquake forces being substantially larger, the responses tend to increase. Figure 9(a–b) display the relative acceleration ($\ddot{x}_*$) and displacement (x_*) of the top floor for 25-storey steel building under the gust wind speed of 46 m/s. It is observed that the addition of stiffness has contradictory impact on the response of the steel buildings. The acceleration ($\ddot{x}_*$) response is observed to increase, whereas, the displacement response is significantly decreased. Similarly, for the base shear (V_b) response, the SBF is observed to have the highest response, which is directly related to the acceleration response of the structure.

Figure 10 presents the inter-storey drift (δ) under the considered wind excitations. It is observed that the stiffness induced passive devices (SB and VED) are effective in controlling the storey drift. Overall, the considered peak responses of the buildings analyzed under the dynamic seismic and wind loadings are plotted in Figure 11 to understand the trend in response quantities and a possible case of multi-hazard scenario. There exist specific circumstances as both the ground motion and gusty wind excitations govern the modal responses, thereby demonstrating a possible example of a multi-hazard situation. Therefore, such contradictory effects of the retrofitting systems have necessitated careful selection of the retrofit solution and design for a structure, duly considering the multi-hazard assessment.

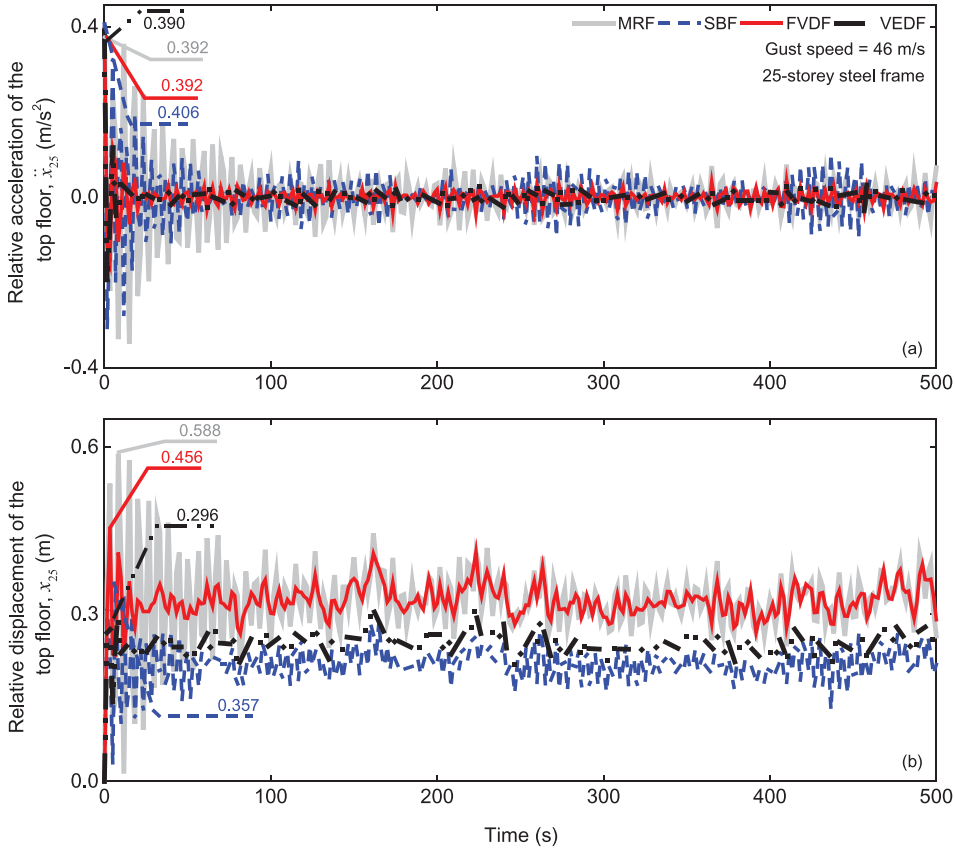

Figure 9. Relative acceleration and displacement of the top floor for 25-storey steel building under the gust wind speed of 46 m/s.

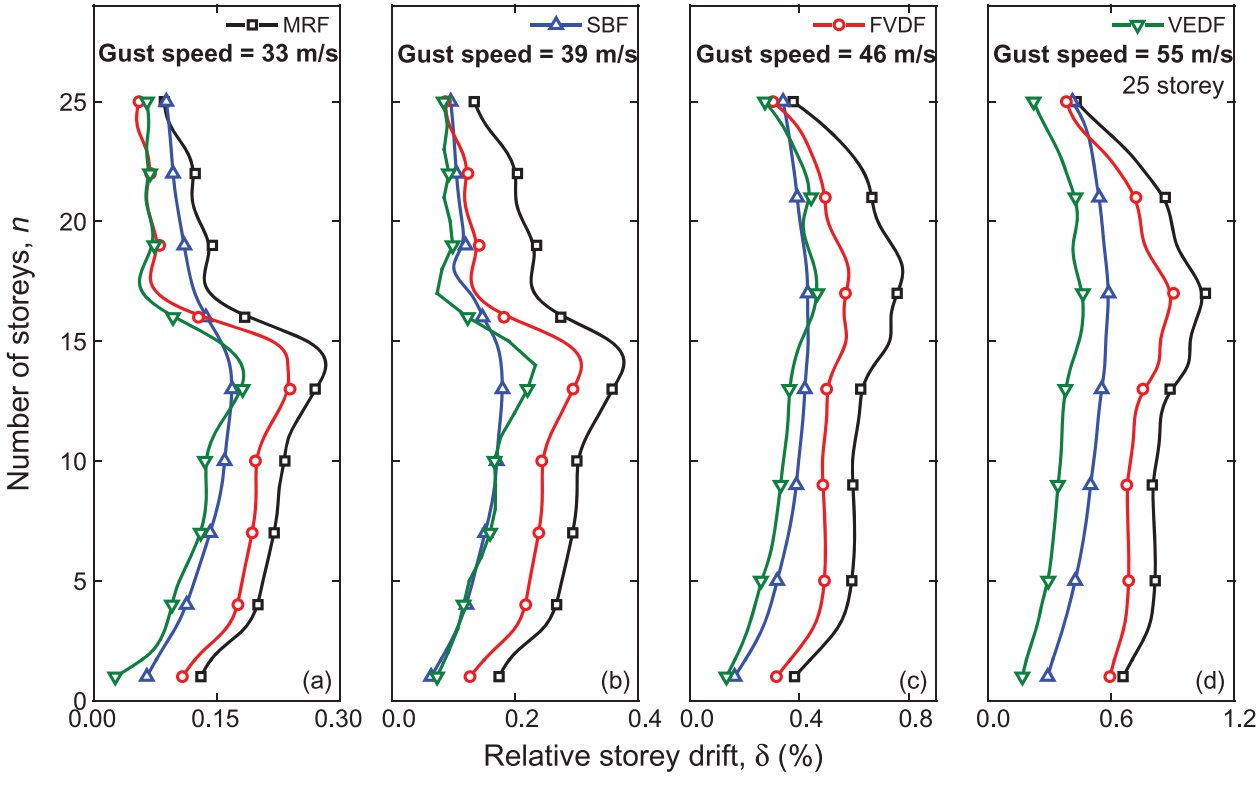

Figure 10. Relative inter-storey drift for the 25-storey steel building under the selected winds.

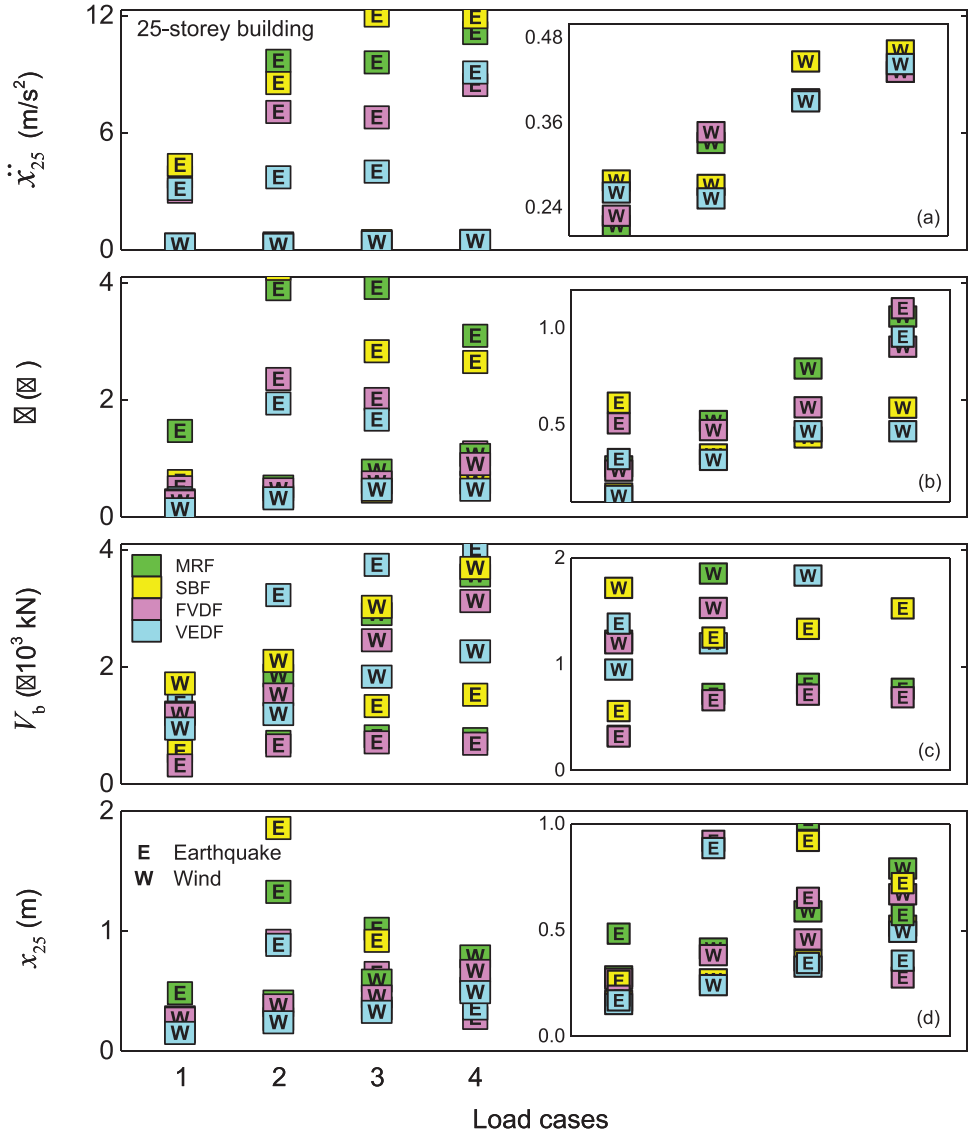

Figure 11. Distribution of the peak load of responses for the 25-storey steel building under the multiple hazard scenarios of earthquake and wind.

5. Multi-Hazard assessment of steel buildings

Herein, the multi-hazard scenario of the steel buildings installed with passive control devices is discussed under the earthquake and wind hazards. The effectiveness of the passive control devices installed in the steel buildings is investigated through the distribution of the peak response data under the considered excitations. To analyze the multi-hazard situation arising from the selection of a retrofitting device in minimizing large forces, specific cases are undertaken to justify the assumption. Column base shear (V_b) and top floor displacement (x_*) responses are selected to examine the validity of the theory. The possible reason of neglecting the other response quantities is that the top floor acceleration and inter-storey drift are directly related to column base shear and displacement, respectively.

The multi-hazard situation is further assessed by defining a limit state, for which the responses are compared against the multiple hazards. The base shear under typical wind loads generally vary from 2 to 6% of the inertial weight of the structure (W) (Paulson, 2004). Therefore, a limit of 0.03 W is adopted, assuming the condition that the response above the limit is considered to worsen, as shown in Figures 12(a)–14(a). The relative displacement is also studied under earthquakes and winds, and therefore, a limit displacement of 0.002 h (h/500) is considered as per any standard provision, where, h is the height of the building, which demarcates the worsening feature when the response is above the limit, as presented in Figures 12(b)–14(b). From Figures 12 and 13, it is noticed that the seismic responses dominate the design of the steel buildings using the passive control devices, as the wind responses are insignificant. However, the retrofitted buildings do not display any worsening feature under the wind loadings.

The 25-storey steel building is assessed for the multi-hazard performance, as shown in Figure 14. The 25-storey building is identified to be governed by both the seismic ground motions and gusty winds. The modal responses of this building frame are contained within a frequency bandwidth influenced by both the hazards. The contradicting behavior under both the non-simultaneous occurring hazards becomes a concern to assess the proper retrofit solutions in exposed regions where

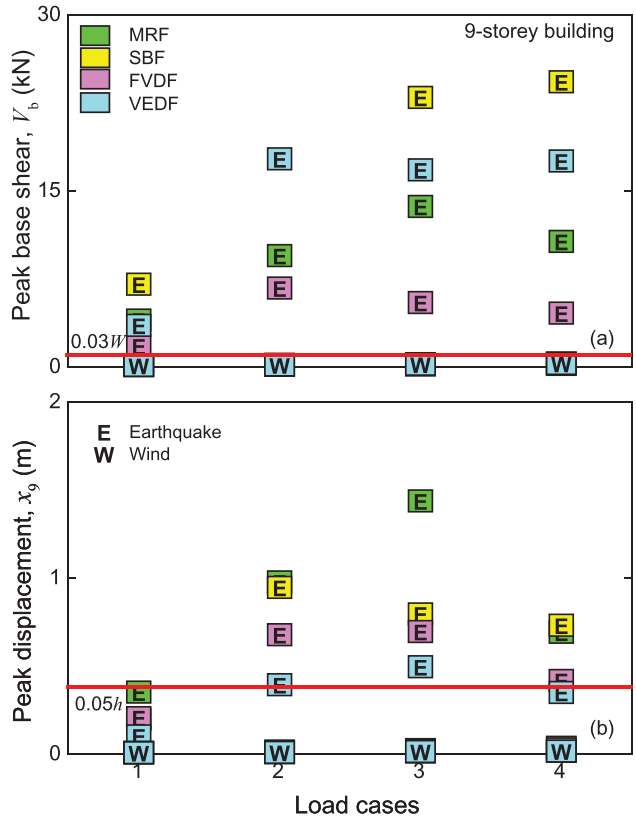

Figure 12. Distribution of the peak: (a) base shear and (b) top floor displacement for the 9-storey steel building under the earthquakes and winds showing limit for response worsening.

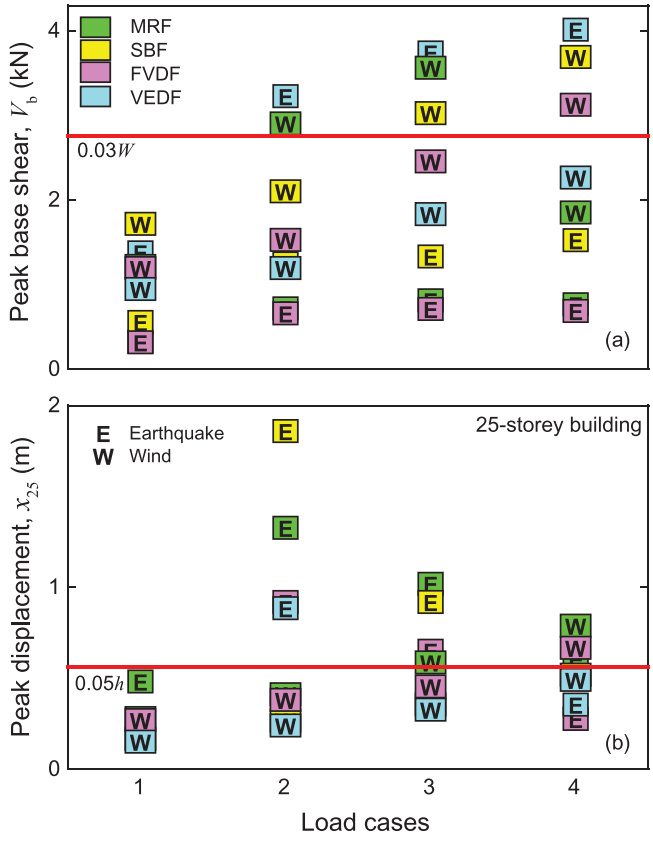

Figure 14. Distribution of the peak: (a) base shear and (b) top floor displacement for the 25-storey steel building under the earthquakes and winds showing limit for response worsening.

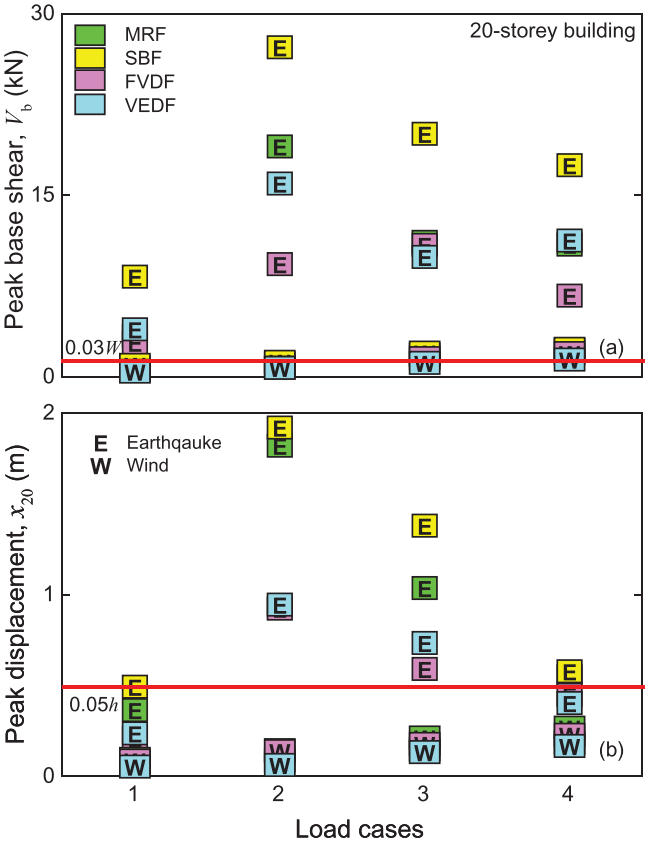

Figure 13. Distribution of the peak: (a) base shear and (b) top floor displacement for the 20-storey steel building under the earthquakes and winds showing limit for response worsening.

multiple hazards predominate. The base shear response is studied under the multiple excitations and it is concluded that the dynamic wind forces govern the design of steel buildings. A close observation on the response indicates that the steel building retrofitted using the VED under wind scenario, induce considerable catastrophic demand under the seismic ground motions.

As a wind load governed structure, several controlled responses under the wind are above the limit state; however, significant response reduction is obtained by using the VED. However, the VEDF response under the earthquake is substantially above the limit, indicating a worsening feature of the retrofit strategy against the earthquake hazard. The modified dynamic properties in this situation act against the favorable conditions of the dissipating devices under the earthquakes. Therefore, it is certain that the benefit reported for a passive control device may prove to be a hindrance against the other hazard, requiring special attention for such critical assessment.

Similar to the base shear, the top floor displacement is reported to have a multi-hazard contradiction under the exciting forces. It is obvious that several seismic response quantities fail based on the criterion considered. However, it is noticed that the seismic response control is ineffective to control the wind response for higher gust speed. The retrofitting strategy, which was supposed to alleviate the response under the larger earthquake loads, became unsuitable for the wind loads. The current scenario is intended to draw significant attention of researchers to develop robust techniques, which could counter the devastating effects of the

hazards occurring in design life of the structures. Thenceforth, a clear vision is required to assess the structures and provide retrofit solutions in such scenarios where the multiple hazards pose significant threat in the design life of structures, which calls for the need to investigating the structures from the multi-hazard perspective.

6. Conclusions

Herein, a multi-hazard assessment is conducted for the 9-, 20- and 25-storey steel buildings by using different stiffness and damping induced retrofitting devices under the dynamic excitations of site-specific earthquakes and winds. The following conclusions are derived from the context of the multi-hazard assessment conducted for the steel buildings:

1. The stiffness induced control devices are ineffective in providing significant seismic response control due to the changed dynamic properties. However, such control devices are mostly capable of reducing the wind response, as the modified properties turn in favor under the wind excitations.
2. The retrofitting strategy supposed to alleviate the response under the lesser wind loads, became unsuitable for the larger earthquake loads. Therefore, it becomes a demanding task to form a judgmental notion in selecting a retrofit device for the structures prone to devastating effects of predominant multiple hazards as earthquake and wind.
3. There exists cases as both the seismic ground motion and gusty wind excitations govern the modal responses, thereby demonstrating a possible example of a multiple hazard situation. These precarious situations arise as the modal frequencies of the structures lie in the frequency bandwidth of the earthquake and wind spectra.
4. In general, it becomes a concern to assess the proper retrofit solutions in exposed regions where multiple hazard predominate. Subsequently, a clear vision is required to assess the structures and provide retrofit solutions in such scenarios where the multiple hazards pose significant threat in the design life of structures, which calls for the need to investigating the structures from the multi-hazard perspective.

Disclosure statement

No potential conflict of interest was reported by the authors.

ORCID

Tathagata Roy http://orcid.org/0000-0002-7238-8142
Vasant Matsagar http://orcid.org/0000-0002-7600-0520

References

Akiyama, M., & Frangopol, D. M. (2013). *Life-cycle design of bridges under multiple hazards: Earthquake, tsunami, and continuous deterioration*. 11th International Conference on Structural Safety and Reliability (ICOSSAR). New York, NY.

Aly, A. M., & Abburu, S. (2015). On the design of high-rise buildings for multi-hazard: Fundamental differences between wind and earthquake demand. *Shock and Vibration*, *2015*, 1. Article number: 148681.

Cha, E. J., & Ellingwood, B. R. (2013). *Acceptance of risk due to competing wind and earthquake hazards*. 11th International Conference on Structural Safety and Reliability (ICOSSAR). New York, NY.

Chandrasekaran, S., & Banerjee, S. (2015). Retrofit optimization for resilience enhancement of bridges under multi-hazard scenario. *Journal of Structural Engineering*, *142*(8), C4015012.

Chao, S.-H., Karki, N. B., & Sahoo, D. R. (2013). Seismic behavior of steel buildings with hybrid braced frames. *Journal of Structural Engineering*, *139*(6), 1019–1032.

Decò, A., & Frangopol, D. M. (2011). Risk assessment of highway bridges under multiple hazards. *Journal of Risk Research*, *14*(9), 1057–1089.

Dogruel, S., & Dargush, G. (2008). *A framework for multi-hazard design and retrofit of passively damped structures. AEI Conference, Building Integration Solutions*, Denver, CO.

Dong, Y., & Frangopol, D. M. (2016). Probabilistic time-dependent multi-hazard life-cycle assessment and resilience of bridges considering climate change. *Journal of Performance of Constructed Facilities*, *30*(5), 04016034.

Duthinh, D., & Simiu, E. (2010). Safety of structures in strong winds and earthquakes: Multi-hazard considerations. *Journal of Structural Engineering*, *136*(3), 330–333.

Elias, S., Matsagar, V., & Datta, T. K. (2017). Distributed tuned mass dampers for multi-mode control of benchmark building under seismic excitations. *Journal of Earthquake Engineering*. DOI: 10.1080/13632469.2017.1351407.

Fur, L.-S., Yang, H. T. Y., & Ankireddi, S. (1996). Vibration control of tall buildings under seismic and wind loads. *Journal of Structural Engineering*, *122*(8), 948–957.

Heydarinouri, H., & Zahrai, S. M. (2017). Iterative step-by-step procedure for optimal placement and design of viscoelastic dampers to improve damping ratio. *Structural Design of Tall and Special Buildings*, *26*(9), e1361.

Jalayer, F., Asprone, D., Prota, A., & Manfredi, G. (2011). Multi-hazard upgrade decision making for critical infrastructure based on life-cycle cost criteria. *Earthquake Engineering & Structural Dynamics*, *40*(10), 1163–1179.

Kalkan, E., & Chopra, A. K. (2010). *Practical guidelines to select and scale earthquake records for nonlinear response history analysis of structures*. USGS Open-File Rep. 2010–1068, 126, By: Erol Kalkan and Anil K. Chopra https://doi.org/10.3133/ofr20101068 ⟨http://nsmp.wr.usgs.gov/ekalkan/MPS/index.html⟩ (June 2010).

Kaur, N., Matsagar, V. A., & Nagpal, A. K. (2012). Earthquake response of mid-rise to high-rise buildings with friction dampers. *International Journal of High-Rise Buildings*, *1*(4), 311–332.

Komendantova, N., Mrzyglocki, R., Mignan, A., Khaza, B., Wenzel, F., Patt, A., & Fleming, K. (2014). Multi-hazard and multi-risk decision-support tools as a part of participatory risk governance: feedback from civil protection stakeholders. *International Journal of Disaster Risk Reduction*, *8*, 50–67.

Kwon, D., & Kareem, A. (2006). *NatHaz on-line wind simulator (NOWS): Simulation of Gaussian multivariate wind fields* (NatHaz Modeling Laboratory Report). University of Notre Dame, Notre Dame, IN.

Lee, D., & Taylor, D. P. (2001). Viscous damper development and future trends. *Structural Design of Tall Buildings*, *10*(5), 311–320.

Lewandowski, R., & Pawlak, Z. (2011). Dynamic analysis of frames with viscoelastic dampers modelled by rheological models with fractional derivatives. *Journal of Sound and Vibration*, *330*(5), 923–936.

Li, Y., & Ellingwood, B. R. (2009). Framework for multi-hazard risk assessment and mitigation for wood-frame residential construction. *Journal of Structural Engineering*, *135*(2), 159–168.

Li, Y., Ahuja, A., & Padgett, J. E. (2012). Review of methods to assess, design for, and mitigate multiple hazards. *Journal of Performance of Constructed Facilities*, *26*(1), 104–117.

Mahmoud, H., & Cheng, G. (2016). Framework for lifecycle cost assessment of steel buildings under seismic and wind hazards. *Journal of Structural Engineering*, *143*(3), 04016186.

Martinez-Rodrigo, M., & Romero, M. L. (2003). An optimum retrofit strategy for moment resisting frames with nonlinear viscous dampers for seismic applications. *Engineering Structures*, *25*(7), 913–925.

Matsagar, V. A., & Jangid, R. S. (2005). Viscoelastic damper connected to adjacent structures involving seismic isolation. *Journal of Civil Engineering and Management*, *11*(4), 309–322.

Mazza, F., & Labernarda, R. (2017). Structural and non-structural intensity measures for the assessment of base-isolated structures subjected to pulse-like near-fault earthquakes. *Soil Dynamics and Earthquake Engineering*, *96*, 115–127.

Mazza, F., & Vulcano, A. (2011). Control of the earthquake and wind dynamic response of steel-framed buildings by using additional braces and/or viscoelastic dampers. *Earthquake Engineering & Structural Dynamics*, *40*(2), 155–174.

Naeim, F. (1998). Performance of 20 extensively-instrumented buildings during the 1994 Northridge earthquake. *Structural Design of Tall Buildings*, *7*(3), 179–194.

Ohtori, Y., Christenson, R. E., Spencer, B. F., & Dyke, S. J. (2004). Benchmark problems in seismically excited nonlinear buildings. *Journal of Engineering Mechanics*, *130*(4), 366–385.

Patel, C. C., & Jangid, R. S. (2011). Dynamic response of adjacent structures connected by friction damper. *Earthquake and Structures*, *2*(2), 149–169.

Paulson, C. (2004). *Seismic versus wind design base shear forces in eastern and mid-western United States*. 13th World Conference on Earthquake Engineering (13WCEE), Vancouver, British Columbia, Canada.

Potra, F. A., & Simiu, E. (2009). Optimization and multi-hazard structural design. *Journal of Engineering Mechanics*, *135*(12), 1472–1475.

Raut, B. R., & Jangid, R. S. (2014). Seismic analysis of benchmark building installed with friction dampers. *IES Journal Part A: Civil and Structural Engineering*, *7*(1), 20–37.

Roy, T., & Agarwal, P. (2016). Comparison of damage index and fragility curve of RC structure using different Indian standard codes. *SERC Journal of Structural Engineering*, *43*(1), 1–9.

Roy, T., & Matsagar, V. (2017). *Multi-hazard assessment of steel buildings retrofitted with passive control devices*. 16th World Conference on Earthquake Engineering, Santiago, Chile.

Samali, B., & Kwok, K. C. S. (1995). Use of viscoelastic dampers in reducing wind- and earthquake-induced motion of building structures. *Engineering Structures*, *17*(9), 639–654.

Seible, F., Hegemier, G., Karbhari, V. M., Wolfson, J., Arnett, K., Conway, R., & Baum, J. D. (2008). Protection of our bridge infrastructure against man-made and natural hazards. *Structure and Infrastructure Engineering*, *4*(6), 415–429.

Sigtryggsdóttir, F. G., Snaebjörnsson, J. T., Grande, L., & Sigbjörnsson, R. (2016). Interrelations in multi-source geo-hazard monitoring for safety management of infrastructure systems. *Structure and Infrastructure Engineering*, *12*(3), 327–355.

Soong, T. T., & Spencer, B. F. (2000). Active, semi-active and hybrid control of structures. *Bulletin of the New Zealand Society for Earthquake Engineering*, *33*(3), 387–402.

Spencer, B. F., Christenson, R. E., & Dyke, S. J. (1999). *Next generation benchmark control problems for seismically excited buildings*. 2nd World Conference on Structural Control, New York, NY.

Tapia, C., & Padgett, J. E. (2016). Multi-objective optimization of bridge retrofit and post-event repair selection to enhance sustainability. *Structure and Infrastructure Engineering*, *12*(1), 93–107.

Venkittaraman, A., & Banerjee, S. (2014). Enhancing resilience of highway bridges through seismic retrofit. *Earthquake Engineering & Structural Dynamics*, *43*(8), 1173–1191.

Yilmaz, T., Banerjee, S., & Johnson, P. A. (2016). Performance of two real-life California bridges under regional natural hazards. *Journal of Bridge Engineering*, *21*(3), 04015063.